High-pressure Brillouin scattering of the single-crystal $PbSc_{1/2}Ta_{1/2}O_3$ relaxor ferroelectric

H. Marquardt,[1] N. Waeselmann,[2] M. Wehber,[2] R. J. Angel,[3] M. Gospodinov,[4] and B. Mihailova[1,*]

[1]*Helmholtz-Zentrum Potsdam, Deutsches GeoForschungsZentrum GFZ, Telegrafenberg, 14473 Potsdam, Germany*

[2]*Fachbereich Geowissenschaften, Universität Hamburg, Grindelallee 48, 20146 Hamburg, Germany*

[3]*Dipartimento di Geoscienze, Universita degli studi di Padova, via G. Gradenigo 6, 35131 Padova, Italy*

[4]*Institute of Solid State Physics, Bulgarian Academy of Sciences, Blvd. Tzarigradsko Chaussee 72, 1784 Sofia, Bulgaria*

(Received 30 November 2012; revised manuscript received 4 March 2013; published 21 May 2013)

The effect of pressure on the acoustic modes and adiabatic elastic constants of the perovskite-type (ABO_3) relaxor compound $PbSc_{1/2}Ta_{1/2}O_3$ have been studied by Brillouin spectroscopy at room temperature up to 9.2 GPa. It is shown that the elastic constants are very sensitive to the pressure-induced structural transformations that were established by diffraction and Raman scattering analysis. Changes in the evolution of the pseudocubic elastic constants c_{11} and c_{44} occur at the two phase-transition pressures $p_{c1} = 1.9$ GPa and $p_{c2} \sim 5.5$ GPa. Changes in evolution of c_{12} occur at the two characteristic pressures $p_1{}^* = 1.2$ GPa and $p_2{}^* \sim 3.0$ GPa, which mark changes in the local structure that precede the corresponding phase transitions. The elastic anisotropy and the width of the transverse acoustic mode increase in the pressure range between p_{c1} and p_{c2} with a maximum near $p_2{}^*$. A strong decrease in the Cauchy parameter is observed at pressures above $p_2{}^*$, which indicates an enhancement of the covalent character of chemical bonding. Increasing pressure gradually suppresses the central peak typical of the relaxor ergodic state, and the quasielastic scattering vanishes at a pressure slightly above $p_2{}^*$.

DOI: 10.1103/PhysRevB.87.184113 PACS number(s): 77.80.Jk, 78.35.+c, 63.20.−e, 62.50.−p

I. INTRODUCTION

Lead-based perovskite-type (ABO_3) relaxor ferroelectrics are technologically important materials, exhibiting remarkably large dielectric permittivities as well as excellent electroelastic and electro-optical properties.[1] Relaxors have also been attracting great attention from a fundamental point of view due to the complexity of their local structure and dynamics responsible for the outstanding properties.[2,3] Relaxors are characterized by a broad and frequency-dependent maximum of the dielectric permittivity as a function of temperature, which results from the existence of dynamic polar nanoregions flipping between different orientation states. Brillouin spectroscopic studies of Pb-based relaxors at different temperatures revealed that the coupling between the polarization fluctuations is accompanied by damping of the acoustic phonon modes and anomalies in the elastic constants.[4–9] Furthermore, recent acoustic emission experiments showed that in the vicinity of the temperature of the dielectric permittivity maximum, an acoustic signal is released that exhibits a nontrivial V-type dependence on the dc electric field.[10–12] This observation can be explained in terms of the coexistence of intermediate-range ferroelectric and antiferroelectric orders[13] that can, respectively, evolve into long-range ferroelectric order on cooling or into long-range antiferrodistortive order under high pressure.[14–16] A competitive coexistence of ferroelectric and antiferrodistortive local distortions in relaxors was also suggested on the basis of inelastic neutron scattering.[17] Hence, the analysis of the pressure dependence of the acoustic phonon modes, in addition to studies at different temperatures, can help provide deeper insights into the complex atomic structure of relaxors. The pressure-induced structural transformations in relaxors have been thoroughly investigated by x-ray and neutron diffraction as well as by Raman spectroscopy,[16,18–24] but high-pressure Brillouin-scattering studies are scarce.[25,26] It was found that the elastic constants of $PbMg_{1/3}Nb_{2/3}O_3$ (PMN), which at room temperature is in a relaxor ergodic state, exhibit an abrupt change at 4.5 GPa,[25] which according to diffraction analysis is the phase-transition pressure from a relaxor-cubic to a rhombohedral structure.[18] On the other hand, for $PbSc_{1/2}Nb_{1/2}O_3$ (PSN), which at room temperature is in a ferroelectric state, a softening and damping of the longitudinal acoustic (LA) mode was observed near 2 GPa, which was attributed to a pressure-induced ferroelectric-paraelectric phase transition, implying that the high-pressure phase of PSN is cubic,[26] in contrast to the case of PMN. The LA mode in pure and $PbTiO_3$-diluted PSN as well as in $PbSc_{1/2}Ta_{1/2}O_3$ (PST) indeed softens and broadens near the Curie temperature,[7,9] but high-pressure diffraction and Raman-spectroscopic studies on both PSN and PST[27–31] complemented by density-functional-theory (DFT) calculations[16] revealed that the high-pressure structure is ferroic, and it is comprised of long-range-ordered octahedral tilts. The similarities between the high-pressure features detected by x-ray diffraction and Raman scattering for $PbB'_{1/3}B''_{2/3}O_3$ (Refs. 18,19,21, and 24) and $PbB'_{1/2}B''_{1/2}O_3$ (Refs. 16 and 23) suggest that all Pb-based perovskite-type relaxors follow nearly the same pattern of structural transformations at high pressures and that the chemistry and stoichiometry only influence the actual values of critical pressures. However, the ambient-pressure elastic anisotropies of PMN (which is of the $PbB'_{1/3}B''_{2/3}O_3$ type) and PST (which is of the $PbB'_{1/2}B''_{1/2}O_3$ type) show different changes with temperature,[8] which emphasize the importance of studying the high-pressure behavior of the elastic constants of various relaxor compounds in order to improve our knowledge of the structure-property relationships.

Both PST and PSN have the stoichiometry $PbB'_{1/2}B''_{1/2}O_3$, and at room temperature undergo a series of pressure-induced structural transformations.[16] However, the critical and characteristic pressures for PST are lower than the corresponding values for PSN, which is beneficial for experiments and makes PST a preferred model compound. In addition, at room temperature PST is in an ergodic state, like PMN

(stoichiometry $PbB'_{1/3}B''_{2/3}O_3$) which would facilitate the comparison between relaxors of different stoichiometric types. In PST, at an intermediate characteristic pressure $p_1{}^* = 1.2$ GPa, the off-centered displacements of Pb and B cations in the polar nanoregions decouple, the B-site cations start to move back to the octahedral centers, and the dynamical long-range order of antiphase BO_6 tilts is developed.[16,27,29] These structural changes on the mesoscopic scale are followed by a continuous phase transition at $p_{c1} = 1.9$ GPa from a cubic phase to a nonpolar rhombohedral phase with an octahedral tilt pattern $a^-a^-a^-$ (Glazer notation).[32] At a second intermediate characteristic pressure $p_2{}^* \sim 3.0$ GPa, unequal octahedral tilts are locally developed, and at $p_{c2} \sim 5.5$ GPa a second phase transition takes place, which involves the development of long-range mixed octahedral tilts $a^+b^-b^-$ and antipolar Pb displacements. In order to follow the pressure dependence of the elastic constants and to determine the extent to which the acoustic modes are involved in the pressure-induced structural transformations of relaxors, we have applied high-pressure Brillouin spectroscopy to chemically disordered PST as a model compound.

II. EXPERIMENTAL DETAILS

Chemically and optically homogeneous single crystals of PST from the same synthesis batch as the samples thoroughly studied by x-ray diffraction, neutron diffraction, and Raman spectroscopy[14,16,27,29] were measured by Brillouin spectroscopy. Following the approach of Stenger and Burggraaf,[33] the degree of long-range chemical 1:1 B-site order of our PST sample was determined by powder x-ray diffraction to be $\rho_{\text{measured}}/\rho_{\text{fully ordered}} = 0.13$, where $\rho = I(111)/I(200)$ and $I(hkl)$ is the integrated area of the corresponding hkl Bragg diffraction peak with Miller indices given in $Fm\bar{3}m$. The mean size of chemically ordered domains determined by applying the Scherrer equation to the 111 Bragg peak is ~6.4 nm.[23] The dielectric permittivity exhibits a broad frequency-dispersive maximum, which for 100 Hz is near 277 K at ambient pressure.[13] A specimen sized ~50 × 50 μm^2 was polished parallel to a cubic {100} plane down to a thickness of approximately 30 μm for high-pressure Brillouin scattering experiments. The sample was loaded in a Boehler-Almax-type diamond anvil cell,[34] using diamonds with a culet diameter of 600 μm, a stainless steel gasket with an initial thickness of 200 μm preindented to 90 μm, and a 4:1 methanol-ethanol mixture as a pressure-transmitting medium that ensures hydrostaticity up to 9.8 GPa.[35] The ruby-line luminescence method[36] was used to determine the hydrostatic pressure p with an uncertainty of approximately 0.1 GPa.

The experiments were carried out with the Brillouin spectroscopic system at the German Research Center for Geosciences. The system consists of a Nd:YVO_4 solid-state laser operating at a wavelength of 532 nm and a Sandercock-type tandem six-pass Fabry-Perot interferometer equipped with a photomultiplier tube for signal detection.[37] The free spectral range of the spectrometer was 24.98 GHz. The measurements were performed in symmetric platelet forward-scattering geometry, where the angle θ between incident and scattered laser beam was set to 60° (see Fig. 1). The relation between the acoustic phonon velocities υ and the measured

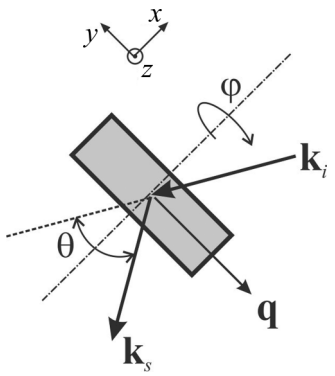

FIG. 1. Sketch of the experimental symmetric platelet forward-scattering geometry used in the study; $\mathbf{k}_i$, $\mathbf{k}_s$, and $\mathbf{q}$ indicate the wave vectors of the incident photon, scattered photon, and the acoustic phonon, respectively. The angle θ was kept at 60°. The rotation angle φ was varied between 0° and 180°. The x, y, and z axes show the initial orientation ($\varphi = 0°$) of the cubic ⟨100⟩ crystallographic directions of the sample (gray rectangle).

frequency shifts $\Delta\nu_\theta$ is then given by[38]

$$\upsilon = \lambda_0 \Delta\nu_\theta / (2\sin(\theta/2)), \tag{1}$$

where λ_0 is the incident laser wavelength (in air). The sample was rotated from 0° to 180° around the compression axis of the diamond anvil cell, which in our experiment coincided with a cubic ⟨100⟩ of the sample, and Brillouin measurements were performed at steps of 10°–15°, thereby sampling several phonon propagation directions in a cubic {100} plane of PST. The collected spectra were fitted using pseudo-Voigt peak shape functions. Elastic constants c_{ijkl} and acoustic velocities are related by the Christoffel equation for nonpiezoelectric media:[39]

$$|c_{ijkl}e_j e_l - \rho\upsilon^2\delta_{ik}| = 0, \tag{2}$$

where δ_{ik} is the Kronecker delta symbol, e_j, e_l are the unity vectors along the corresponding acoustic-wave propagation directions q_j, q_l, and ρ is the sample mass density. An inversion procedure based on the Christoffel equation[40] was then used to determine the elastic constants from acoustic velocities measured at different rotation angles φ (see Fig. 1). The density of PST at each pressure value was calculated from a polynomial interpolation of high-precision pressure-volume (p-V) experimental data previously measured by single-crystal x-ray diffraction.[27]

Additional Brillouin scattering measurements were performed with the free spectral range of the spectrometer set to 149.90 GHz and a prolonged acquisition time of ~1 h to follow the pressure dependence of the central spectral feature near 0 GHz.

III. RESULTS AND DISCUSSION

A representative high-pressure Brillouin spectrum of PST collected with a free spectral range of 24.98 GHz is shown in Fig. 2(a). The three pairs of Stokes/anti-Stokes (S/AS) peaks correspond to the sample LA, sample transverse acoustic (TA) and pressure medium (PM) acoustic modes. Two propagating TA phonon modes with polarizations perpendicular to each

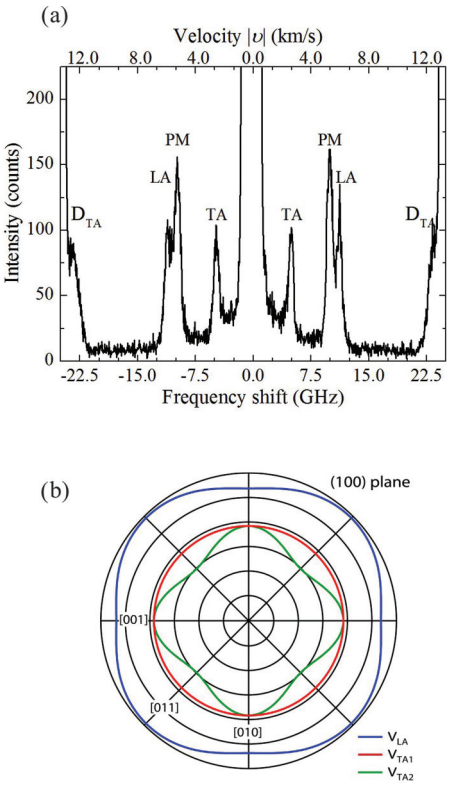

FIG. 2. (Color online) (a) Representative Brillouin spectrum of PST measured with a free spectral range of 24.98 GHz at $p = 5.9$ GPa and at a rotation angle $\varphi = 60°$; LA, TA, PM, and D_{TA} refer to sample LA, sample transverse, PM, and diamond TA modes, respectively, and (b) A sketch of the (100) cross section of the velocity surface of the acoustics modes in an elastically anisotropic cubic crystal. Due to elasto-optic coupling, the TA mode exhibiting an isotropic (circular) distribution of the velocity is not detected in our experiments.

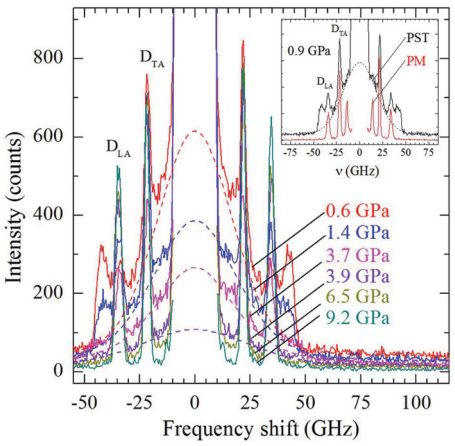

FIG. 3. (Color online) Selected representative spectra measured at different pressures with a free spectral range of 149.90 GHz, revealing the presence of an intense quasielastic central feature at pressures $\leqslant$3.7 GPa, which appears as extended wings on the elastic-scattering peak centered at 0 GHz; D_{TA} and D_{LA} designate the AS peaks originating from the diamond acoustic transverse and longitudinal modes, respectively. The inset shows the spectra collected at 0.9 GPa from the sample (PST) and alongside the sample (PM), demonstrating that the methanol-ethanol PM does not contribute to the central feature. The dashed lines represent pseudo-Voigt functions fitted to the quasielastic scattering. The spectrum of PST at 3.9 GPa could be fitted equally well with and without an additional central peak at 0 GHz; no additional central peak was required to fit the spectra of PST at 6.5 and 9.2 GPa.

other are generally expected in solids, and in elastically anisotropic cubic crystals the cross section of the velocity surface of one TA mode is circular in the {100} planes [see Fig. 2(b)], while the other TA mode as well as the LA mode shows a pronounced anisotropy. Due to elasto-optic coupling effects, the TA phonon with a circular cross section of the velocity surface is not visible in our scattering geometry. The diamond anvils produce strong Brillouin scattering near 23 GHz.

For relaxors, the ambient-pressure scattering peak at 0 GHz is comprised of both elastic Rayleigh scattering and a quasielastic scattering component (central peak) that originates primarily from the flipping of polar nanoregions.[8,9,41] For PST, the temperature dependence of the central peak at ambient pressure shows a broad anomaly near the temperature of the dielectric permittivity maximum T_m and a sharp anomaly at 290 K.[8,41] The latter temperature matches very well the characteristic temperature T_n attributed to antiferroelectric ordering on the mesoscopic scale,[13] which suggests that dynamic antiferrodistortive species may also contribute to the central peak. Figure 3 shows selected Brillouin spectra of PST measured with a free spectral range of 149.90 GHz at pressures between 0.6 and 9.2 GPa. The quasielastic scattering gives rise to the extended tail on the peak centered at 0 GHz that is clearly visible in the low-pressure spectra but is absent from the high-pressure spectra (Fig. 3). Comparison of the spectra collected at the same pressure from the sample and from the PM (the inset of Fig. 3) clearly shows that this central feature observed at low pressures is generated by the sample. The quasielastic scattering gradually decreases in intensity when the pressure is increased up to 3.7 GPa and becomes negligible or vanishes at higher pressures. To verify this trend, the spectral profiles were fitted with pseudo-Voigt functions $PV = qL + (1-q)G$, $q \in [0,1]$, in which L is Lorentzian and G is Gaussian. The positions of the PV functions used for the strong Rayleigh (elastic) scattering and for the central peak (quasielastic scattering) were fixed to zero, but no other constraints were used during the fittings. In all spectra the PV function used to model the Rayleigh scattering exhibited a negligible Lorentzian component ($q \leqslant 0.012$) and a full width at half maximum (FWHM) close to 6 GHz. The central peak was fitted either with a variable q parameter or with a pure Lorentzian but this did not influence the pressure trend of the integrated intensity. The fittings confirmed that at 6.5 and 9.2 GPa, there is no additional zero-positioned peak related to quasielastic scattering. The spectrum measured at 3.9 GPa could be fitted equally well with and without an additional zero-positioned peak, but the refined intensity of such a peak is very weak, exhibits very large uncertainty, and it is strongly correlated with the other fitting parameters. These results indicate that, within the experimental uncertainties, the quasielastic scattering disappears near 3.9 GPa, which can also be deduced from the pressure trend of the normalized intensity of the central peak (Fig. 4). Up to 3.9 GPa, the width

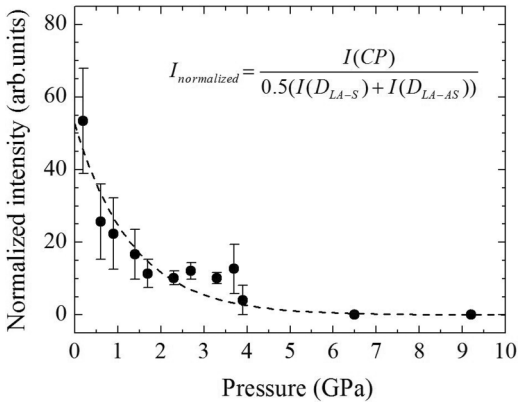

FIG. 4. Pressure dependence of the intensity of the central peak $I(CP)$ normalized to the average intensity of the LA-S and LA-AS peaks of diamond obtained from fitting the spectral profiles with pseudo-Voigt functions. The error bars in the normalized intensities are calculated from the uncertainties in intensities obtained from the fits to the spectral profiles. Note that the true uncertainties may be larger due to the unavoidable effects of focusing differences between measurements, which would affect the ratio between the contribution from the sample and from the diamond anvils. The dashed line is merely a guide for the eye, representing a simple exponential decay fit to the data points.

of the central peak remains the same within uncertainties. Previous x-ray diffraction experiments showed that the diffuse x-ray scattering generated by polar nanoregions is strongly suppressed at $p_{c1} = 1.9$ GPa, although it does not completely disappear.[23,27] Therefore, the detection of a central peak above p_{c1} may be related to the different sensitivity of Brillouin spectroscopy compared to x-ray diffraction, but the existence of other dynamic ferroic species up to 3.9 GPa cannot be ruled out.

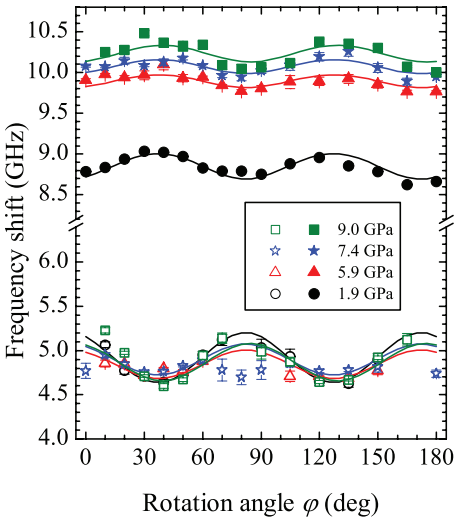

FIG. 5. (Color online) Angular dependence of the frequency shifts of the LA (solid symbols) and TA modes (open symbols) at 1.9 GPa (circles), 5.9 GPa (triangles), 7.4 GPa (stars), and 7.4 GPa (squares) obtained from unconstrained fits to the spectral profiles. The lines represent best-fit models assuming cubic symmetry.

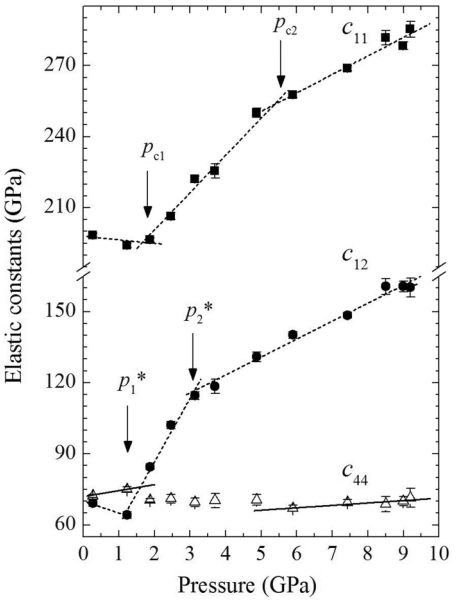

FIG. 6. Pressure dependence of the pseudocubic elastic constants c_{11} (solid squares), c_{12} (solid circles), and c_{44} (open triangles). The dashed lines are linear fits to the c_{11} and c_{12} data in the corresponding pressure ranges. The solid lines are linear fits to the c_{44} data points below 2 GPa and above 5 GPa. The arrows mark the characteristic and critical pressures determined independently by diffraction and Raman scattering.[16,27,29]

Figure 5 shows an example of the angular dependence of the velocities υ_{LA} and υ_{TA} measured at relatively low and high pressure, along with the least-square fits obtained assuming cubic symmetry. For a perfectly oriented (100)-plate of a cubic crystal measured in symmetric scattering geometry, the phonon propagation direction is in the (100) plane, and thus the dependence of the acoustic velocities on the rotation angle should exhibit a 90° periodicity with the maxima and minima of both υ_{LA} and υ_{TA} corresponding to wave propagation in the direction of the cubic crystallographic axes [see the sketch in Fig. 2(b)]. This behavior is indeed observed for the LA velocity measured at all pressures. Up to 6 GPa, which is well above the first phase transition, the experimental data points for υ_{TA} also follow a cubiclike angular dependence, indicating that the structure remains essentially pseudocubic. Above 6 GPa, some of the measured υ_{TA} values do not match a cubic model, which is presumably due to the enhancement of the ferroic structural distortions. Nevertheless, because the pressure-induced structural distortions detected by neutron diffraction[29] are very small, and in order to make comparison between data easier, cubic point symmetry $m\bar{3}m$ was used for data analysis through the entire pressure range. Hence, the complete set of independent elastic constants under consideration was c_{1111}, c_{1122}, and c_{2323} or, in Voigt-matrix notation, c_{11}, c_{12}, and c_{44}.

The pressure-induced variations of c_{11}, c_{12}, and c_{44} are shown in Fig. 6. The corresponding values at the lowest experimental pressure $p = 0.27 \pm 0.08$ GPa are 198.4 ± 0.9, 69.1 ± 1.3, and 72.2 ± 0.7 GPa. These values are close to the ambient-pressure elastic constants of PST with a low degree of chemical order.[8] The changes with pressure of c_{11} and c_{12},

which, respectively, represent the longitudinal and transverse uniaxial stresses generated by a tensile strain, are similar: initially both c_{11} and c_{12} soften with the pressure increase, then strongly harden, and above a certain pressure the slopes of $c_{11}(p)$ and $c_{12}(p)$ are approximately halved. The pressures at which kinks in $c_{11}(p)$ are observed match very well the two phase-transition pressures $p_{c1} = 1.9$ GPa and $p_{c2} = 5.5$ GPa determined from diffraction and Raman-scattering measurements,[16] whereas the kinks in $c_{12}(p)$ correspond to the two intermediate characteristic pressures $p_1{}^* \sim 1.2$ GPa and $p_2{}^* \sim 3.0$ GPa.[16,27,29] Apparently, c_{12} is more sensitive to the mesoscopic-scale structural changes preceding the alteration of the long-range order, while c_{11} mirrors the transitions of the overall structure. A softening when approaching the first phase transition has also been observed for the isothermal bulk modulus for both phases.[27] Softening of both phases adjacent to structural phase transitions in function of temperature is well known and well understood[42,43] and occurs in perovskite-type materials.[44] At high-pressure transitions, the intrinsic softening due to the structural transformation is superimposed upon the intrinsic hardening due to the increase in pressure and softening in the low-pressure phase is only observed in a few cases.[45] In the case of PST, the initial softening of the structure with pressure increase may be related to the suppression of the coupled off-centered cationic displacements in the polar nanoregions. The strong increase in c_{12} and c_{11} between $p_1{}^*$ and $p_2{}^*$ and between p_{c1} and p_{c2}, respectively, is most probably caused by the enhancement of long-range-ordered antiphase BO_6 tilts of equal magnitude, in the absence of off-centered cations. The reduction of the change in the structural stiffness represented by c_{12} and c_{11} observed above $p_2{}^*$ and p_{c2}, respectively, is most probably related to the development of coupled antipolar Pb shifts, accompanied by an alteration in the octahedral tilt pattern,[16] which occur on the intermediate-range (for c_{12}) and long-range scale (for c_{11}).

The two phase-transition pressures can also be seen in the pressure dependence of c_{44} (Fig. 6), which represents the elastic shear strength along the cubic ⟨100⟩ direction. The elastic constant c_{44} initially increases with the pressure increase and then drops at p_{c1}, indicating that the pressure-induced phase transition from a relaxor ergodic state to a nonpolar rhombohedral phase comprising antiphase octahedral tilts[23,27,29] is associated with the reduction of the shear strength. Between p_{c1} and p_{c2}, c_{44} remains constant, then at p_{c2} drops again, but above p_{c2}, the value of c_{44} starts to increase once more.

The comparison between PMN[25] and PST reveals that for both compounds the shear modulus c_{44} exhibits a similar pressure dependence near the phase transition from a relaxor to a rhombohedral state with antiphase octahedral tilts. The same behavior has been observed for temperature-induced phase transitions from $Pm\bar{3}m$ to $R\bar{3}c$ in other perovskite-type materials.[44] However the elastic constants c_{11} and c_{12} behave differently for PMN and PST, suggesting that the quantity $(c_{11} - c_{12})/2$, which represents the shear modulus for the cubic ⟨110⟩ direction may exhibit a different pressure trend for PMN and PST. Thus, we considered further the pressure dependence of the parameter $A = 2c_{44}/(c_{11} - c_{12})$, describing the ratio between the elastic shear moduli along the cubic edge and the cubic face diagonal in a cubic {100} plane (Zener ratio; Fig. 7).

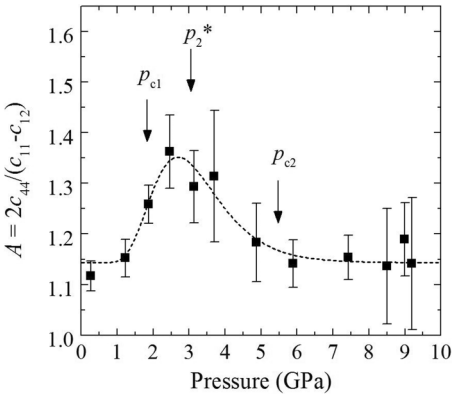

FIG. 7. Pressure dependence of the Zener ratio $A = 2c_{44}/(c_{11} - c_{12})$, which represents the elastic anisotropy of the sample. The arrows mark the characteristic and critical pressures as determined by diffraction and Raman scattering.[16,27,29] The dashed line represents the fit to the experimental data using an asymmetric log-normal function.

This ratio is equal to unity for elastically isotropic media,[39] and thus deviation from unity is indicative of elastic anisotropy. Similar to PMN, the low-pressure Zener ratio of PST is slightly larger than one and increases at the first phase transition. For PST, the increase in A at p_{c1} is smaller than that observed for PMN,[25] indicating that the difference between the shear stiffness along the cubic ⟨100⟩ and ⟨110⟩ is less pronounced for PST than for PMN. In contrast to PMN,[25] a further anomaly in the elastic anisotropy was observed for PST (see Fig. 7): the Zener ratio A decreases when pressure approaches p_{c2}, and above p_{c2} it returns to the ambient-pressure value of ∼1.14. The absence of a second anomaly for PMN in the elastic constants and consequently in the anisotropy is consistent with PMN not exhibiting any further phase transitions up to 10 GPa.[18,22] The pressure dependence of the Zener ratio A measured for PST can be fitted with an asymmetric log-normal function with a mean value of 3.02 ± 0.17 GPa (see Fig. 7), which is indistinguishable from $p_2{}^*$ determined by Raman spectroscopy.[16] The high-pressure phase between p_{c1} and p_{c2} is nonpolar rhombohedral and consists of long-range antiphase BO_6 tilts of the same magnitude along the three cubic [100], [010], and [001] directions.[16,29] Hence, the existence of $a^-a^-a^-$ tilt pattern along with the absence of coupled off-centered cation shifts is most probably the reason for the enlarged elastic anisotropy. It should be noted that, according to DFT calculations, at high pressure the $a^-a^-a^-$ tilt pattern is energetically less stable than the mixed $a^+b^-b^-$ tilt pattern accompanying the Pb antipolar order that is experimentally observed above p_{c2}.[16] Therefore, the second pressure-induced phase transition might be triggered by the excess of elastic anisotropy related to enhanced antiphase octahedral tilting in the absence of ordered cation off-centered shifts. Since $A(p)$ increases by ∼0.2 between p_{c1} and p_{c2}, one can conclude that the accumulation of shear stress along the cubic ⟨100⟩ is in fact more critical than that along ⟨110⟩ for the development of long-range antipolar order of Pb and compatible rearrangements of the oxygen atoms.

In contrast to the case of PSN,[26] the LA mode in PST did not show any damping upon pressure increase in the

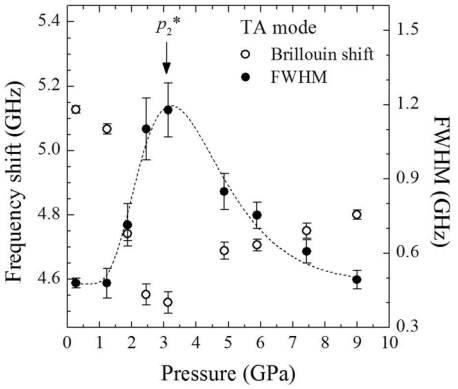

FIG. 8. Pressure dependence of Brillouin shift (triangles) and FWHM (squares) of the TA mode averaged over the rotation angle φ. The error bars are calculated from the uncertainties obtained from the spectrum-profile fittings. The dashed line represents an asymmetric log-normal fit to the experimental data of FWHM. The arrow marks the second characteristic pressure $p_2{}^*$ as determined by Raman scattering.[16,27]

studied pressure range. This is most probably related to the fact that at room temperature, PST is in the cubic relaxor ergodic state, i.e., there is no pressure-induced crossover from a long-range ferroelectric to a cubic paraelectric state as in the case of PSN.[26] The TA mode, however, exhibits softening and damping near the second characteristic pressure $p_2{}^* = 3$ GPa (see Fig. 8). The pressure dependence of the FWHM of the TA mode resembles the $A(p)$ dependence and can also be fit with an asymmetric log-normal function with a global maximum a 3.2 GPa and a mean value 3.79 $\pm$ 0.14 GPa. This indicates that the local development of unequal BO_6 tilts that precedes p_{c2} (Ref. 16) is coupled to the TA mode, i.e., it is related to small periodic fluctuations in the shear strain.

Figure 9 shows the pressure dependence of the pressure-adapted Cauchy parameter $c_{44}/(c_{12} - 2p)$,[46] which has a value of unity for systems with pure central (pairwise) interatomic forces. At ambient conditions the Cauchy parameter of PST is close to unity.[8] With increasing pressure, the Cauchy parameter

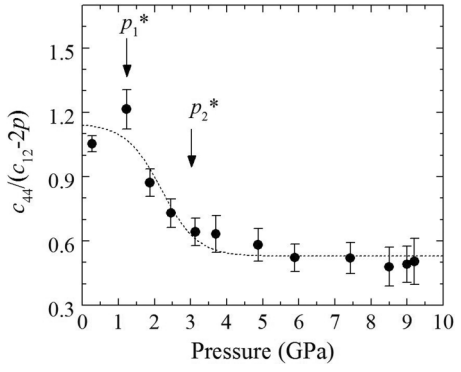

FIG. 9. Pressure dependence of the Cauchy parameter $c_{44}/(c_{12} - 2p)$ indicative of the contribution of noncentral atomic interactions to the crystal potential; the dashed line is a Boltzmann fit to the data and the refined inflection point is 2.19 $\pm$ 0.26 GPa, which is equal to p_{c1} within the uncertainties. The arrows mark the characteristic pressures as determined by diffraction and Raman scattering.[16,27,29]

first slightly increases up to $p_1{}^*$ (see Fig. 9), then rapidly decreases up to $p_2{}^*$, and above 4.0 GPa reaches a saturation value of ~0.5. This suggests that at high pressures noncentral atomic forces contribute significantly to the crystal potential, which indirectly indicates that the cation-oxygen polyhedra are strongly distorted. This is in good agreement with Raman-scattering and diffraction data.[16]

The elastic constants were used to calculate the adiabatic Voigt bulk modulus K_S as well as the average Voigt-Reuss-Hill shear modulus $G_{\mathrm{VRH}} = (G_V + G_R)/2$, where G_V and G_R are, respectively, the Voigt and Reuss average shear moduli. For cubic crystals, $K_S = (c_{11} + 2c_{12})/3$, $G_V = (c_{11} - c_{12} + 3c_{44})/5$, and $G_R = 5/(4s_{11} - 4s_{12} + 3s_{44}) = 5(c_{11} - c_{12})c_{44}/(3c_{11} - 3c_{12} + 4c_{44})$, where s_{11}, s_{12}, and s_{44} are the corresponding elastic compliances.[39] Since the material is close to isotropic in its elastic properties, the values of G_R and G_V for PST are very close to each other, showing a maximum absolute deviation of 1.4 GPa, a difference of just 2.3%. The pressure dependences of K_S and G_{VRH} are shown in Fig. 10. The first phase transition p_{c1} is clearly mirrored by the discontinuous change in both K_S and G_{VRH}. Similar to the corresponding elastic constants, K_S increases at p_{c1}, while G_{VRH} decreases. The second phase transition at p_{c2} is revealed by the change in the slope of $K_S(p)$ as well as the subtle drop in $G_{\mathrm{VRH}}(p)$.

For cubic materials the Voigt bulk modulus, which describes the effect of isotropic strain, is identical with the Reuss bulk modulus $K_{\mathrm{Reuss}} = 1/(3s_{11} + 6s_{12})$, which represents the case

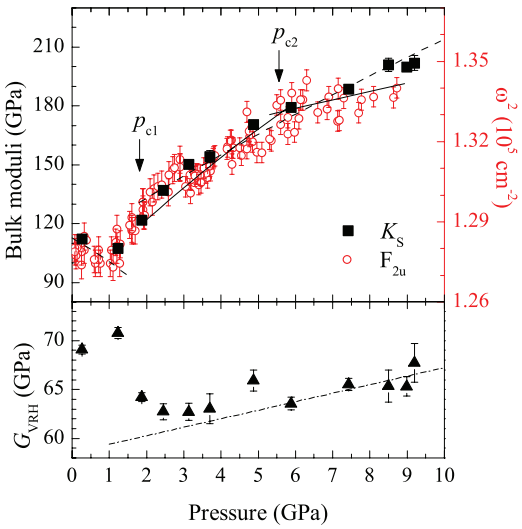

FIG. 10. (Color online) Adiabatic bulk modulus K_S (solid squares) and Voigt-Reuss-Hill shear modulus G_{VRH} (solid triangles) calculated from the elastic constants. The dashed line represents the isothermal bulk modulus K_T calculated from $V(p)$ data,[27] assuming only one phase transition at $p_{c1} = 1.9$ GPa. The solid line is a recalculation of the same $V(p)$ data taking into account the existence of a second phase transition at $p_{c2} \sim 5.5$ GPa, using two independent Birch-Murnaghan equations of state with data ranging from 1.9 to 4.7 GPa and from 5.9 to 8.3 GPa, respectively. The dot-dash line is a linear fit to the high-pressure points for G_{VRH}. The open circles represent the pressure dependence of the square wave number ω^2 of the Raman scattering near 350 cm^{-1} related to the F_{2u} mode of the aristotype cubic structure.[16,27]

of applying isotropic stress, and thus can be compared with the isothermal bulk modulus K_T obtained from compression data measured by single-crystal x-ray diffraction. Figure 10 also depicts the isothermal bulk modulus of PST; the dashed line represents K_T calculated from the equations of state fitted to the experimental p-V data with the assumption for a phase transition only at $p_{c1} = 1.9$ GPa,[27] while the solid line is the recalculated isothermal bulk modulus, taking into account the existence of a second phase transition as later revealed by follow-up studies.[16] As can be seen in Fig. 10, the pressure dependence of the recalculated isothermal bulk modulus obtained from diffraction data is in full agreement with that of the adiabatic bulk modulus obtained from the Brillouin spectroscopic data presented here. It should be emphasized that in the pressure range between p_{c1} and p_{c2} the value of dK/dp is approximately 15. This is a clear indication that the compression of the PST structure involves a significant contribution from noncentral interatomic forces because in systems with negligible noncentral forces, the values of dK/dp are limited to the range of 3.8 to 8.[47] To shed light on the microscopic origin of the large macroscopic stiffening, we reinspected our Raman scattering data from PST.[16,27] Previous Raman scattering analyses revealed that the intensity of the peak near 350 cm^{-1} is strongly enhanced with pressure in all Pb-based relaxor ferroelectrics that have been studied.[16,19,21,23,24] This type of vibration is related to the silent F_{2u} mode of the aristotype cubic structure,[23] which is comprised of vector displacements of oxygen atoms along the Pb-O bonds within planes perpendicular to the cubic body diagonals (see Fig. 11). It can be considered as BO_6 tilting, but the wave number is predominantly determined by the Pb-O stretching force constants.[23] The Raman peak generated by this optical mode is very sensitive to the two intermediate characteristic pressures, as its wave number ω starts to strongly increase at $p_1{}^*$ due to the development of correlated antiphase octahedral tilts of equal magnitude, and then it splits at $p_2{}^*$, indicating the development of unequal BO_6 tilts on the local scale and, respectively, different Pb-O bond lengths. For the sake of comparison, the square wave number ω^2 of the two split components above 3 GPa were averaged, which is essentially an average over the force constants acting in the plane perpendicular to the cubic body diagonal, and the square wave number of the Raman scattering related to the cubic F_{2u} mode was also plotted in Fig. 10. As can be seen, the $\omega^2(p)$ dependence for this optical mode matches very well the pressure dependence of the adiabatic bulk modulus. Hence, the overall crystal volume compressibility is directly related to the local compressibility of the PbO_{12} cavity, which in turn has to accommodate the evolving BO_6 tilting.

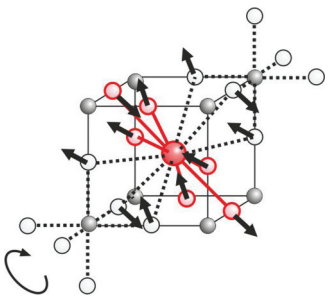

FIG. 11. (Color online) . Sketch of the atomic vector displacements of the silent F_{2u} mode in the aristotype cubic perovskite structure. The large circle represents the A-positioned Pb^{2+} cation, while the small darker and brighter circles represent the B-site cations and oxygen anions, respectively.

IV. CONCLUSIONS

The variation with pressure of the elastic constants of PST obtained by Brillouin scattering shows anomalies in close proximity to the characteristic and critical pressures derived from diffraction analysis and Raman spectroscopy.[16] On compression, the elastic moduli c_{11} and c_{12} as well as the adiabatic bulk modulus K_S first softens due to local changes involving decoupling of off-centered Pb and B-site cations and then strongly hardens in the pressure range in which ordered $a^-a^-a^-$ BO_6 tilts are developed. The rate of hardening is then smaller above the critical pressure, at which long-range-ordered antipolar Pb displacements accompanied by $a^+b^-b^-$ BO_6 tilts appear. The changes in the slope of $c_{12}(p)$ occur at the characteristic pressures of structural alteration on the mesoscopic scale, while $c_{11}(p)$ mirrors the alteration of the global structure. Comparison with the pressure behavior of the optical phonon mode related to Pb-O bond stretching reveals that the global volume compressibility is controlled by the mean local compressibility of the PbO_{12} cavity. The c_{44} elastic constant as well as the average shear modulus drops at p_{c1} and then slowly increases with further pressure increase with a subtle drop at p_{c2}.

The increase in the elastic anisotropy between the two phase-transition pressures $p_{c1} = 1.9$ GPa and $p_{c2} \sim 5.5$ GPa as well as the softening of the TA phonon mode near the second intermediate pressure $p_2{}^* = 3$ GPa suggests that the structural instability developed when approaching p_{c2} is related to BO_6 tilting in the absence of ordered cation off-centered displacements coupled with small fluctuations in the shear strain. At low pressures ($\leqslant p_1{}^*$), the Cauchy parameter is slightly above unity but considerably decreases at high pressures ($> p_2{}^*$), which, along with the large value of $dK/dp \sim 15$, reveals the strong contribution of noncentral forces to the crystal potential, i.e., the covalent character of bonding is enhanced under pressure. Further, the central peak typical of relaxors at ambient conditions gradually disappears as pressure is increased. It still persists above the first critical pressure p_{c1} but disappears above 3.9 GPa, indicating that the dynamic structural fluctuations in PST are suppressed by increasing pressure and they are absent above $\sim$4 GPa.

ACKNOWLEDGMENTS

Financial support by the Deutsche Forschungsgemeinschaft grants (MI 1127/2-2 and SP 1216/3-1) is gratefully acknowledged. The authors thank Sergio Speziale, GeoForschungsZentrum Potsdam, for the fruitful discussions and valuable comments.

*Corresponding author: boriana.mihailova@uni-hamburg.de

[1] L. E. Cross, *in Piezoelectricity: Evolution and Future of a Technology*, edited by W. Heywang, K. Lubitz, and W. Wersing, Vol. 114 (Springer-Verlag, Berlin, 2008), p. 131.

[2] A. A. Bokov, and Z.-G. Ye, J. Mater. Sci. **41**, 31 (2006).

[3] R. A. Cowley, S. N. Gvasaliya, S. G. Lushnikov, B. Roessli, and G. M. Rotaru, Adv. Phys. **60**, 229 (2010).

[4] J.-H. Ko, T. H. Kim, S. Kojima, A. A. Bokov, and Z.-G. Ye, J. Phys.: Condens. Matter **22**, 485902 (2010).

[5] S. G. Lushnikov, A. I. Fedoseev, S. N. Gvasaliya, and S. Kojima, Phys. Rev. B **77**, 104122 (2008).

[6] M. Ahart, A. Hushur, Y. Bing, Z.-G. Ye, R. J. Hemley, and S. Kojima, Appl. Phys. Lett. **94**, 142906 (2009).

[7] S. Kojima, S. Tsukada, Y. Hidaka, A. A. Bokov, and Z.-G. Ye, J. Appl. Phys. **109**, 084114 (2011).

[8] A. I. Fedoseev, S. G. Lushnikov, S. N. Gvasaliya, and S. Kojima, Phys. Solid State **48**, 1102 (2006).

[9] V. Sivasubramanian and S. Kojima, Phys. Rev. B **85**, 054104 (2012).

[10] E. Dul'kin, E. Mojaev, M. Roth, I. P. Raevski, and S. A. Prosandeev, Appl. Phys. Lett. **94**, 252904 (2009).

[11] E. Dul'kin, B. Mihailova, M. Gospodinov, and M. Roth, Europhys. Lett. **94**, 57002 (2011).

[12] E. Dul'kin, B. Mihailova, M. Gospodinov, and M. Roth, J. Appl. Phys. **112**, 064107 (2012).

[13] E. Dulkin, B. Mihailova, G. Catalan, M. Gospodinov, and M. Roth, Phys. Rev. B **82**, 180101(R) (2010).

[14] B. Mihailova, B. Maier, C. Paulmann, T. Malcherek, J. Ihringer, M. Gospodinov, R. Stosch, B. Güttler, and U. Bismayer, Phys. Rev. B **77**, 174106 (2008).

[15] N. Waeselmann, B. Mihailova, B. J. Maier, C. Paulmann, M. Gospodinov, V. Marinova, and U. Bismayer, Phys. Rev. B **83**, 214104 (2011).

[16] B. J. Maier, N. Waeselmann, B. Mihailova, R. J. Angel, C. Ederer, C. Paulmann, M. Gospodinov, A. Friedrich, and U. Bismayer, Phys. Rev. B **84**, 174104 (2011).

[17] I. P. Swainson, C. Stock, P. M. Gehring, Guangyong Xu, K. Hirota, Y. Qiu, H. Luo, X. Zhao, J.-F. Li, and D. Viehland, Phys. Rev. B **79**, 224301 (2009).

[18] B. Chaabane, J. Kreisel, B. Dkhil, P. Bouvier, and M. Mezouar, Phys. Rev. Lett. **90**, 257601 (2003).

[19] J. Kreisel, B. Dkhil, P. Bouvier, and J.-M. Kiat, Phys. Rev. B **65**, 172101 (2002).

[20] S. N. Gvasaliya, V. Pomjakushin, B. Roessli, Th. Strässle, S. Klotz, and S. G. Lushnikov, Phys. Rev. B **73**, 212102 (2006).

[21] P. E. Janolin, B. Dkhil, P. Bouvier, J. Kreisel, and P. A. Thomas, Phys. Rev. B **73**, 094128 (2006).

[22] G.-M. Rotaru, S. N. Gvasaliya, V. Pomjakushin, B. Roessli, Th. Strässle, S. G. Lushnikov, T. A. Shaplygina, and P. Günter, J. Phys.: Condens. Matter **20**, 104235 (2008).

[23] B. Mihailova, R. J. Angel, B. J. Maier, A.-M. Welsch, J. Zhao, M. Gospodinov, and U. Bismayer, IEEE Trans. Ultrason. Ferroelectr. Freq. Control. **58**, 1905 (2011).

[24] N. Waeselmann, B. J. Maier, B. Mihailova, R. J. Angel, J. Zhao, M. Gospodinov, C. Paulmann, N. Ross, and U. Bismayer, Phys. Rev. B **85**, 014106 (2012).

[25] M. Ahart, M. Somayazulu, Z.-G. Ye, R. E. Cohen, Ho-kwang Mao, and R. J. Hemley, Phys. Rev. B **79**, 132103 (2009).

[26] M. Ahart, H.-k. Mao, R. E. Cohen, R. J. Hemley, G. A. Samara, Y. Bing, Z.-G. Ye, and S. Kojima, J. Appl. Phys. **107**, 074110 (2010).

[27] B. Mihailova, R. J. Angel, A.-M. Welsch, J. Zhao, J. Engel, C. Paulmann, M. Gospodinov, H. Ahsbahs, R. Stosch, B. Güttler, and U. Bismayer, Phys. Rev. Lett. **101**, 017602 (2008).

[28] A.-M. Welsch, B. Mihailova, M. Gospodinov, R. Stosch, B. Güttler, and U. Bismayer, J. Phys.: Condens. Matter **21**, 235901 (2009).

[29] B. J. Maier, R. J. Angel, W. G. Marshall, B. Mihailova, C. Paulmann, J. M. Engel, M. Gospodinov, A.-M. Welsch, D. Petrova, and U. Bismayer, Acta Cryst. B **66**, 280 (2010).

[30] B. J. Maier, A.-M. Welsch, R. J. Angel, B. Mihailova, J. Zhao, J. M. Engel, L. A. Schmitt, C. Paulmann, M. Gospodinov, A. Friedrich, and U. Bismayer, Phys. Rev. B **81**, 174116 (2010).

[31] B. J. Maier, R. J. Angel, B. Mihailova, W. G. Marshall, M. Gospodinov, and U. Bismayer, J. Phys.: Condens. Matter **23**, 035902 (2011).

[32] A. M. Glazer, Acta Crystallogr. Sec. B **28**, 3384 (1972).

[33] C. G. F. Stenger and A. F. Burggraaf, Phys. Status Solidi **61**, 275 (1980).

[34] R. Boehler, Rev. Sci. Instrum. **77**, 115103 (2006).

[35] R. J. Angel, M. Bujak, J. Zhao, G. Diego Gatta, and S. D. Jacobsen, J. Appl. Crystallogr. **40**, 26 (2007).

[36] W. B. Holzapfel, J. Appl. Phys. **93**, 1813 (2003).

[37] H. Marquardt, S. Speziale, S. Jahn, S. Ganschow, and F. R. Schilling, J. Appl. Phys. **106**, 093519 (2009).

[38] C. H. Whitfield, E. M. Brody, and W. A. Bassett, Rev. Sci. Instrum. **47**, 942 (1976).

[39] R. E. Newnham, *Properties of Materials* (Oxford University Press, New York, 2005).

[40] A. G. Every, Phys. Rev. B **22**, 1746 (1980).

[41] S. G. Lushnikov, F. M. Jiang, and S. Kojima, Solid Stat. Commun. **122**, 129 (2002).

[42] M. A. Carpenter and E. K. H. Salje, Eur. J. Mineral. **10**, 693 (1998).

[43] P. Toledano, M. M. Fejer, and B. A. Auld, Phys. Rev. B **27**, 5717 (1983).

[44] M. A. Carpenter, S. V. Sinogeikin, and J. D. Bass, J. Phys.: Condens. Matter **22**, 035404 (2010).

[45] J. D. C. McConnell, C. A. McCammon, R. J. Angel, and F. Seifert, Z. Kristallogr. **215**, 669 (2000).

[46] H. Shimizu, H. Tashiro, T. Kume, and S. Sasaki, Phys. Rev. Lett. **86**, 4568 (2001).

[47] A. M. Hofmeister, Geophys. Res. Lett. **20**, 635 (1993).